*Aerosol and Air Quality Research*, 18: 1774–1787, 2018

ISSN: 1680-8584 print / 2071-1409 online
doi: 10.4209/aaqr.2017.10.0396

# A Comparative Analysis of Aerosol Microphysical, Optical and Radiative Properties during the Spring Festival Holiday over Beijing and Surrounding Regions

**Yu Zheng[1,2], Huizheng Che[2*], Xiangao Xia[3], Yaqiang Wang[2], Hujia Zhao[2], Hong Wang[2], Victor Estellés[4], Linchang An[5], Ke Gui[2], Tianze Sun[2], Boshi Kang[6], Deguang Zhang[7], Chunyang Zhao[8], Chong Liu[9], Zhuozhi Shu[1], Yongliang Sun[1], Bingbo Huang[1], Rongfan Chai[1], Tianliang Zhao[1], Xiaoye Zhang[2]**

[1] *Key Laboratory of Meteorological Disaster, Ministry of Education/Joint International Research Laboratory of Climate and Environment Change/Collaborative Innovation Center on Forecast and Evaluation of Meteorological Disasters/Key Laboratory for Aerosol-Cloud-Precipitation of China Meteorological Administration, Nanjing University of Information Science and Technology, Nanjing 210044, China*
[2] *State Key Laboratory of Severe Weather (LASW) and Institute of Atmospheric Composition, Chinese Academy of Meteorological Sciences, CMA, Beijing 100081, China*
[3] *Laboratory for Middle Atmosphere and Global Environment Observation (LAGEO), Institute of Atmospheric Physics, Chinese Academy of Sciences, Beijing 100029, China*
[4] *Departament de Física de la Terra i Termodinàmica, Universitat de València, 46100 Burjassot Valencia, Spain*
[5] *National Meteorological Center, CMA, Beijing 100081, China*
[6] *Meteorological Equipment Support Center, Liaoning Meteorological Bureau, Shenyang 110016, China*
[7] *Inner Mongolia Institute of Meteorology Sciences, Inner Mongolia Meteorological Bureau, Hohhot 010051, China*
[8] *Meteorological Observatory, Shenzhen Meteorological Bureau, Shenzhen 518040, China*
[9] *School of Atmospheric Sciences, Nanjing University, Nanjing 210093, China*

## ABSTRACT

Using ground-based data, meteorological observations, and atmospheric environmental monitoring data, a comparative analysis of the microphysical and optical properties, and radiative forcing of aerosols was conducted between three stations in different developed environments during a severe air pollution episode during the Spring Festival over Beijing. During the most polluted period, the daily peak values of the aerosol optical depth were ~1.62, ~1.73, and ~0.74, which were about 2.6, 2.9, and 2.1 times higher than the background levels at the CAMS, Xianghe, and Shangdianzi sites, respectively. The daily peak values of the single scattering albedo were ~0.95, ~0.96, and ~0.87. The volume of fine-mode particles varied from 0.04 to 0.21 $\mu m^3\ \mu m^{-2}$, 0.06 to 0.17 $\mu m^3\ \mu m^{-2}$, and 0.01 to 0.10 $\mu m^3\ \mu m^{-2}$, which were about 0.3 to 5.8, 1.1 to 4.7, and 1.2 to 8.9 times greater than the background values, respectively. The daily absorption aerosol optical depth was ~0.01 to ~0.13 at CAMS, ~0.03 to ~0.14 at Xianghe, and ~0.01 to ~0.09 at Shangdianzi, and the absorption Ångström exponents reflected a significant increase in organic aerosols over CAMS and Xianghe and in black carbon over Shangdianzi. Aerosol radiative forcing at the bottom of the atmosphere varied from –20 to –130, –40 to –150, and –10 to –110 W $m^{-2}$ for the whole holiday period, indicating the cooling effect. The potential source contribution function and concentration-weighted trajectory analysis showed that Beijing, the southern parts of Hebei and Shanxi, and the central northern part of Shandong contributed greatly to the pollution.

***Keywords:*** Air pollution; Aerosol optical properties; Radiative forcing; Spring Festival holiday; Beijing.

## INTRODUCTION

Aerosol particles influence regional and global climate change by scattering or absorbing radiant energy, thereby affecting the earth's radiation budget (Ackerman *et al.*, 1981; Nakajima *et al.*, 1990; Charlson *et al.*, 1992; Hansen *et al.*, 2000; Takamura *et al.*, 2004; Wang *et al.*, 2010; Gui

* Corresponding author.
*E-mail address:* chehz@cma.gov.cn

*et al.*, 2017; Che *et al.*, 2018). Moreover, aerosol particles can play a role as cloud condensation nuclei, altering the size distribution of cloud droplets, affecting their physical characteristics, and contributing to change in cloud precipitation efficiency (Nakajima *et al.*, 1996; Dubovik *et al.*, 2000; Campanelli *et al.*, 2012; Eck *et al.*, 2012; Estellés *et al.*, 2012). Despite numerous studies on aerosol particles, there is still much uncertainty surrounding aerosol optical properties in relation to current assessments and predictions of regional and global climatic change (Takamura *et al.*, 1994; Nakajima *et al.*, 2001; Ramanathan *et al.*, 2001; Estellés *et al.*, 2007).

Aerosol particles not only contribute to global and regional climate change, but can also cause environmental and public health problems (Wang *et al.*, 2006; Zhang *et al.*, 2013; Zhao *et al.*, 2013). Over the last 30 years, rapid economic and societal growth in China has led to substantial changes in human activities, such as industrialization, urbanization, and increasing car numbers (Ge *et al.*, 2009; Zhao *et al.*, 2009; Xin *et al.*, 2014). As a result, high concentrations of aerosol particles are found in many megacities (Qiu and Yang, 2000; Luo *et al.*, 2001; Li *et al.*, 2013; Zhao *et al.*, 2015), resulting in a reduction in both visibility and the penetration of solar radiation (Watson *et al.*, 2002; Che *et al.*, 2005; Che *et al.*, 2007; Wang *et al.*, 2008; Gui *et al.*, 2016), and a deterioration in air quality (Wang *et al.*, 2003; Zheng *et al.*, 2016), especially in the North China Plain (Xia *et al.*, 2005; Xue *et al.*, 2011; Zhu *et al.*, 2014).

The study of aerosol optical properties is useful in increasing our understanding of air pollution (Garland *et al.*, 2008; Zhang *et al.*, 2008; Wang *et al.*, 2011; Chen *et al.*, 2014; Che *et al.*, 2015), and several studies in recent years have focused on megacities such as Beijing. Eck *et al.* (2010) analyzed fine- and coarse-mode aerosol particles over Beijing and stated that the fine-mode particles showed a negative correlation with single scattering albedo (SSA) when the fine-mode particle content was less than 50%. Xue *et al.* (2011) suggested that both the increasing amount of dry pollution aerosols and the enhanced hygroscopic growth of the aerosol contributed greatly to the total atmospheric extinction coefficient based on a study about the influences of pollution particles on the optical properties near Beijing. Che *et al.* (2014) studied the optical and radiative properties of aerosol during a serious haze-fog pollution episode in the North China Plain and found that during the pollution stage, the fine-mode aerosol optical depth (AOD) was about 2.5 times bigger than that during the non-pollution stage at urban sites in Beijing. However, relatively few studies have focused on the aerosol optical properties in this area during the Spring Festival holiday, considering the unique human activities and pollution emission conditions that occur at this time (Huang *et al.*, 201; Yu *et al.*, 20132; Jing *et al.*, 2014; Jiang *et al.*, 2015; Zheng *et al.*, 2017). During the Spring Festival, there are intensive and widespread fireworks as the people celebrate the Chinese New Year, and this offers an opportunity to study the influences of human activities on optical and radiative properties of aerosol.

The primary purpose of this study was to investigate the variational characteristics of aerosol microphysical, optical and radiative properties at three sites (representative of urban, suburban, and rural environments) in the Beijing and surrounding regions using a CE-318 sun-photometer, including AOD, Ångström exponent (α), SSA, and aerosol volume size distributions, which could be affected by human activities during this traditional holiday. This work not only provides a preliminary view of aerosol optical properties during this holiday period, but is also conducive to increasing our knowledge on the influence of human activities on air pollution, which would contribute to improving regional air quality.

## SITES, DATA AND ANALYTICAL METHODS

### *Site Descriptions and Instrumentation*

Three sites in the Beijing and surrounding regions, with available solar- and sky-scanning radiometer (Cimel Electronique CE-318) measurements, were selected for this study (Fig. 1). Table 1 shows the geographical details and site descriptions. The observation station at the Chinese Academy of Meteorological Sciences (CAMS) is located in the central urban area of Beijing, and the main pollution sources are originated from urban activities (Zheng *et al.*, 2016). Xianghe is a suburban station, located 50 km east of Beijing, and its measurements show the aerosol characteristics of a suburban area in Beijing (Xia *et al.*, 2005). The Shangdianzi rural site is located 150 km to the northeast of Beijing, and is considered a regional atmospheric background station because it is far away from large anthropogenic emission sources (Che *et al.*, 2014).

The Cimel Electronique CE-318 sun photometer has eight channels at 1640, 1020, 870, 670, 500, 440, 380, and 340 nm, and the 940 nm water vapor channel with a 1.2° field of view (Holben *et al.*, 1998). The sun photometers at the CAMS and Xianghe sites are operational within both CARSNET (China Aerosol Remote Sensing Network) and AERONET (Aerosol Robotic Network) (Che *et al.*, 2008), and were calibrated with AERONET-PHOTONS calibration (Holben *et al.*, 1998) at Lille University (LOA/USTL, France) and Izaña Observatory (Tenerife, Spain). Calibration of the sun photometers at the Shangdianzi site followed the calibration protocol used by AERONET, and inter-comparison and sphere calibrations were performed every year by CARSNET to ensure the accuracy of the measurements (Tao *et al.*, 2014). This study analyzed the optical parameters of aerosols (using level 1.5 data with the cloud screening), including the AOD, Ångström exponent (α), SSA, absorption AOD (AAOD), absorption Ångström exponent (AAE), volume size distribution, and radiative forcing.

### *Analytical Methods and Data*

In this study, the Chinese Spring Festival holiday in 2016 was selected to investigate the influences of human activities on optical and radiative properties of aerosol. For comparison, we used two-month-average value (including the holiday period) to illustrate the general background level at each observation site.

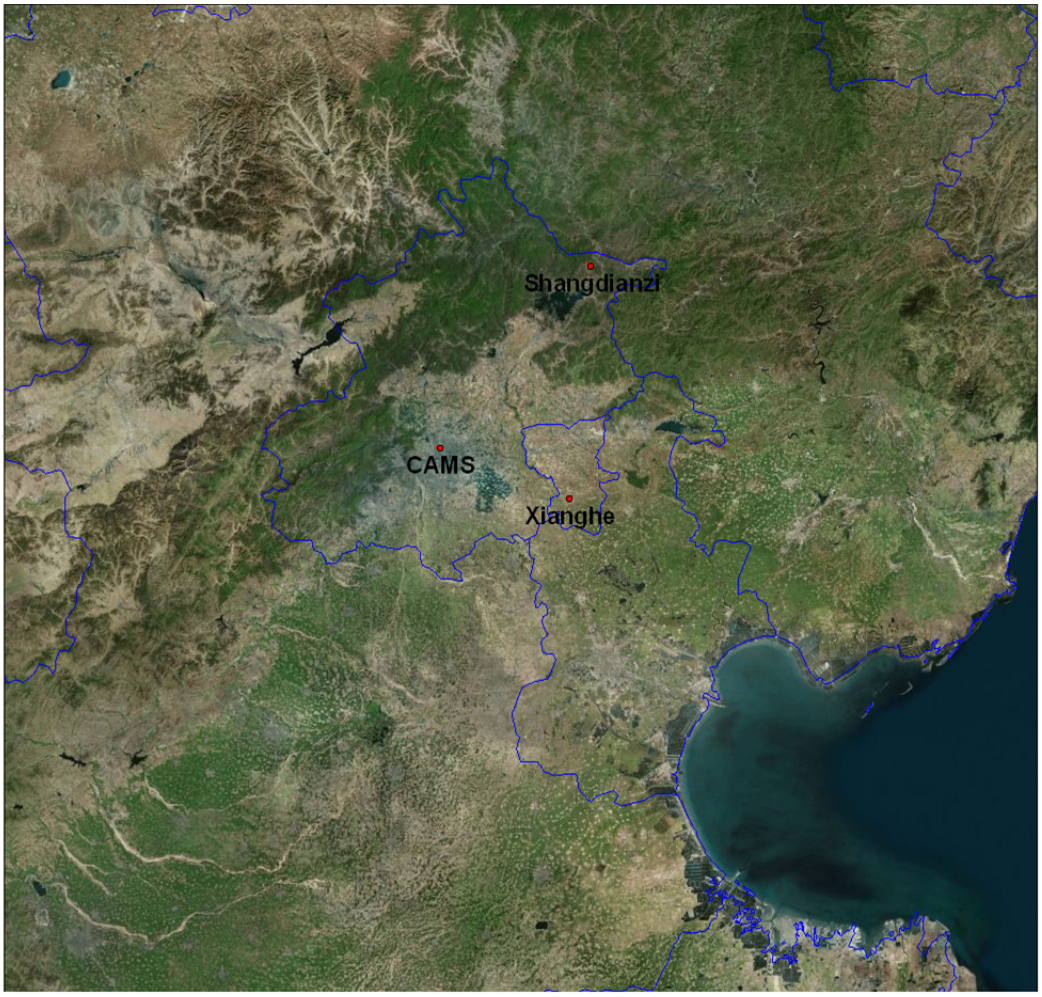


**Fig. 1.** Distribution of the three sun photometer sites.

**Table 1.** Description of urban sites in this study.

| Station name | Latitude (°N) | Longitude (°E) | Elevation | Location |
|---|---|---|---|---|
| CAMS | 39.93 | 116.32 | 106 m a.s.l. | central Beijing |
| Xianghe | 39.75 | 116.96 | 36 m a.s.l. | 50 km E of Beijing |
| Shangdianzi | 40.65 | 117.12 | 393 m a.s.l. | 150 km NE of Beijing |

Surface meteorological data and vertical observation data during the study period were obtained from the China Meteorological Administration, and the hourly particulate matter (PM) concentration data were obtained from the China National Environmental Monitoring Centre (http://www.cnemc.cn/). There are about 30 monitoring stations located in Beijing. We calculated the average value of all these stations to obtain a representative value of the entire $PM_{2.5}$ mass concentration over the Beijing region for this study (Che *et al.*, 2014). ERA-Interim data (global reanalysis datasets, http://apps.ecmwf.int/datasets) were used to analyze the regional variation in the surface wind field and the height of the planetary boundary layer. Version 4 of the Hybrid Single Particle Lagrangian Integrated Trajectory (HYSPLIT) model (Draxler and Hess, 1998) was used to track the transport pathways of air masses arriving during the haze event.

This study used potential source contribution function (PSCF) analysis and this technique has often been used to identify the probable locations of emission sources affecting pollutant loadings in this study area (Yan *et al.*, 2015; Xin *et al.*, 2016). The concentration-weighted trajectory (CWT) method, developed by Hus *et al.* (2003), was used to distinguish between strong and weak sources and show the probable contributions. Detailed information about this method, including the algorithm and principle, has been reported previously (Stohl, 1996; Polissar *et al.*, 2001) and is thus not repeated here.

## RESULTS AND DISCUSSION

### *Meteorological Conditions and Pollutant Concentrations*

*Analysis of Meteorological and PM Data*

The temporal variation of the concentrations of PM and

the meteorological conditions at the three sites were investigated before analyzing the optical properties of the aerosols. This was because these two factors make a substantial contribution to the air pollution. Fig. 2 shows the time series of PM concentrations at these three sites (the dash line shows the mean value, and so are the follows). Fig. 3 illustrates the daily mean variation in the surface wind field and planetary boundary layer height (PBLH) over the Beijing region. The wind direction can affect the transport of air pollutants and may dominate the spatial distribution of visibility. The wind speed also has a substantial influence on the accumulation and diffusion of aerosol particles, and thus is an important factor affecting the concentration of PM (Che *et al.*, 2007). The PBLH plays a significant role in determining the vertical distributions of aerosol particles, because the higher the accumulation of ambient aerosols, the less solar radiation reaches the surface, which will further restrict the development of the planetary boundary layer, thus compounding the air pollution near the surface during stable weather conditions (Deardorff *et al.*, 1972; Gao *et al.*, 2015; Leng *et al.*, 2015).

It is clear from Fig. 2 that the daily $PM_{2.5}$ mass concentration varied coincidentally with the $PM_{2.5}/PM_{10}$ ratio. About 10 days before the Spring Festival holiday began (27–29 January), an air pollution event occurred, during which the daily mean PM mass concentrations were higher than background levels (~53 μg $m^{-3}$), with a maximum of ~125 μg $m^{-3}$ observed on 28 January. During

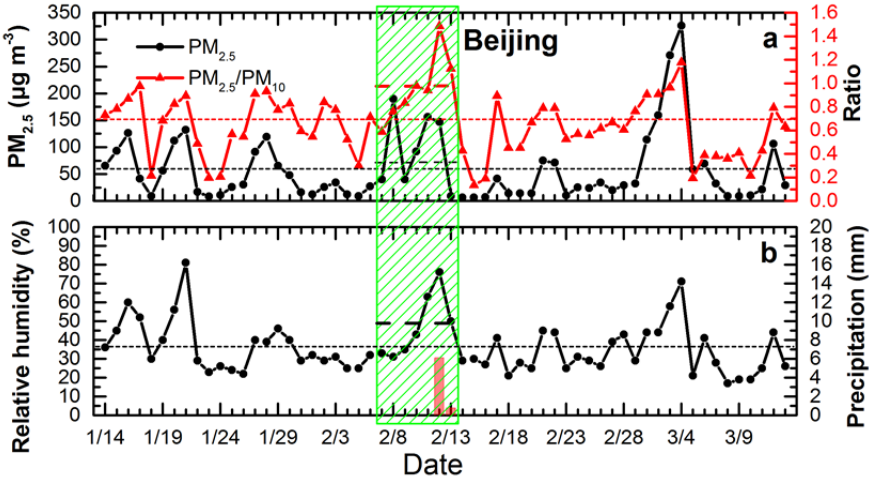


**Fig. 2.** Daily variation in particle mass concentrations, the ratio of $PM_{2.5}$ to $PM_{10}$, and the humidity, in Beijing.

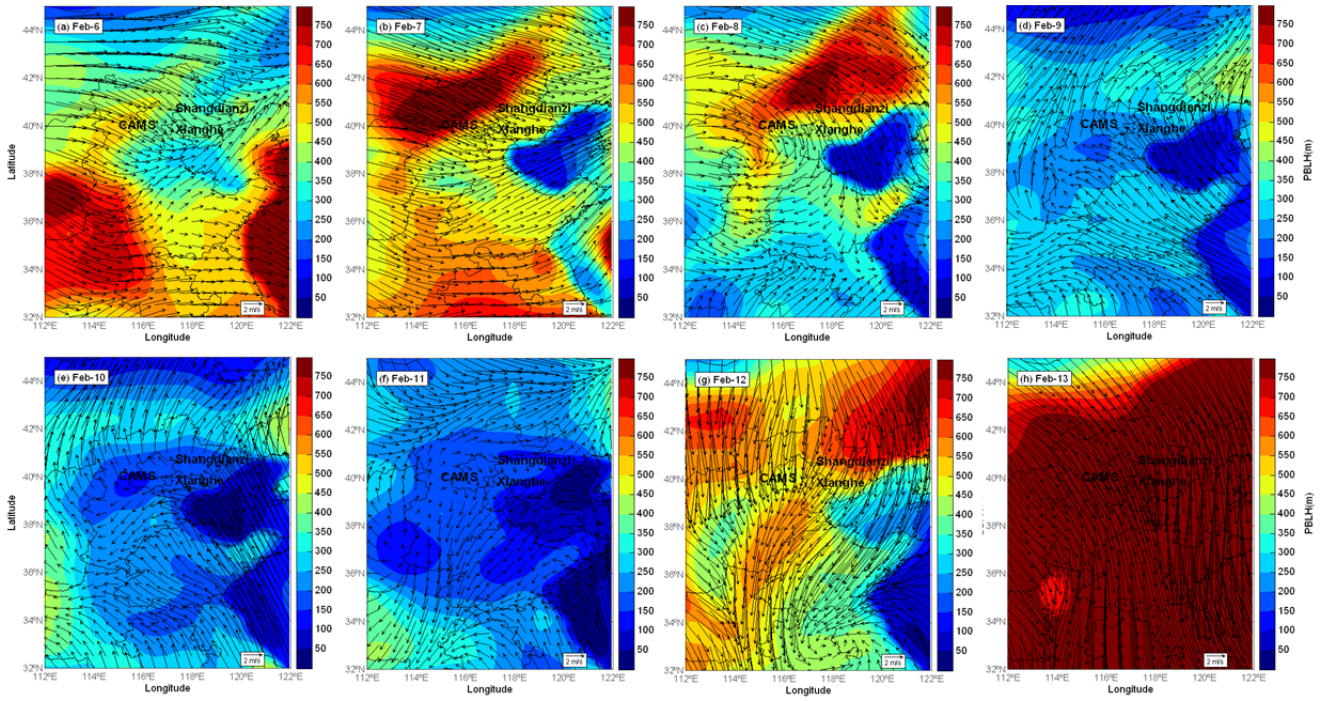


**Fig. 3.** Daily average wind field at the surface and the PBLH over the Beijing region from 6 to 13 February (ERA-Interim dataset).

these three days, the $PM_{2.5}/PM_{10}$ ratios were almost ~0.9, indicating the generation of numerous fine aerosol particles. Following this, the daily PM mass concentrations and the $PM_{2.5}/PM_{10}$ ratio showed a decreasing trend and the $PM_{2.5}$ values fell below the background level.

During the holiday, serious air pollution episodes were observed on 8 February and 10–12 February, with $PM_{2.5}$ concentrations higher than 150 μg $m^{-3}$. The mean $PM_{2.5}$ concentration and the $PM_{2.5}/PM_{10}$ ratio during the holiday period was ~65 μg $m^{-3}$ and ~1.0, which were about 23% and 43% higher than the background levels (~53 μg $m^{-3}$ and ~0.7), respectively. As can be seen from Fig. 3, when the severe air pollution began (10–12 February), the weather conditions on the day before shared the same characteristics (9–11 February), showing weak southerly surface winds (lower than 2 m $s^{-1}$) and relatively low PBLH (~200 m), which impeded the diffusion of atmospheric pollutants. Another pollution episode occurred about 8 days after the holiday (21–22 February), with a $PM_{2.5}$ concentration and $PM_{2.5}/PM_{10}$ ratio of ~67 μg $m^{-3}$ and ~0.8, which were about 27% and 14% higher than the background levels, respectively.

In general, the variation in relative humidity (RH) was similar to that of $PM_{2.5}$ (Fig. 2(b)), which generally showed relatively high values during the air pollution episodes. During the holiday air pollution period (10–12 February), the RH increased with the $PM_{2.5}$ concentrations, and reached a maximum (~80%) on 12 February. The mean RH value over the holiday period was ~49%, which was about 36% higher than the background level (~36%). It should be noted that the RH affects the hygroscopic growth of fine-mode aerosol particles (Che *et al.*, 2014; Fu *et al.*, 2014). Furthermore, the high humidity conditions strongly enhanced the formation of secondary aerosol species such as $NO_3^-$, $SO_4^{2-}$, and secondary organic compounds, in a similar manner to the processes occurring in clouds (Blando *et al.*, 2000; Hennigan *et al.*, 2008).

*Analysis of Atmospheric Stratification of Temperature*

The continuous inversion of temperature near the surface in the vertical direction is conducive to the accumulation of air pollutants. This is because a stable thermal structure restricts the vertical motion of air masses, reducing the diffusion of pollutants to higher altitudes, and eventually leading to pollution being confined near to ground level (Fu *et al.*, 2014).

Fig. 4 shows the vertical distribution of temperature in Beijing from 6 till 13 February 2016. It is clear that the surface temperature inversion layer was almost continuous, having been observed at both 0800 h and 2000 h (local time) during the entire holiday, especially when the air pollution was serious. In addition, during the period of 10–12 February, when the air pollution was most severe, the temperature inversion layer not only occurred near the ground (~100 m), but was also observed in the upper atmosphere (~750 m), indicating that weak vertical motion of air masses occurred during these days, favoring the accumulation of air pollutants near the ground, and contributing to the high pollution episode.

## *Optical Properties of Aerosols*

*AOD, Ångström Exponent and Water Vapor*

As can be seen from the spatial and temporal variation of

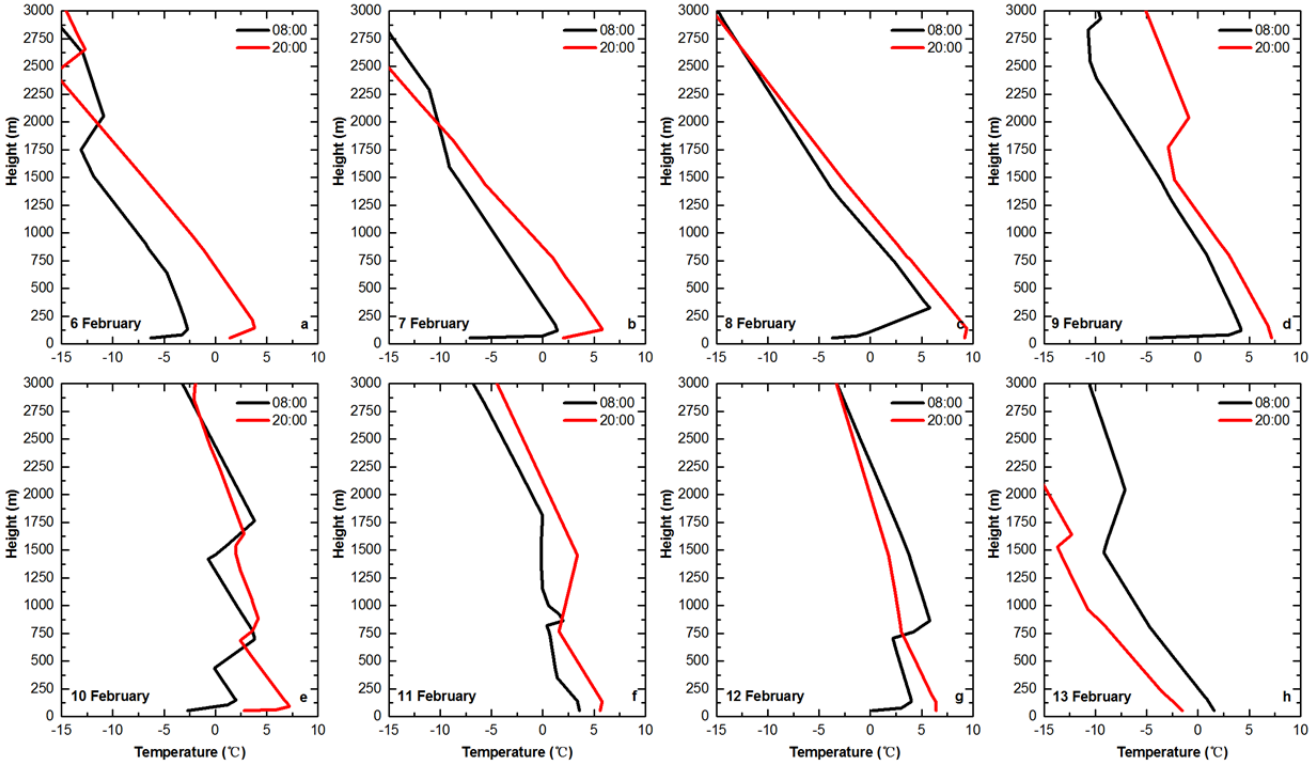


**Fig. 4.** Vertical distribution of temperature over Beijing during the holiday period.

the AOD at 440 nm and $\alpha_{440-870}$ nm in Fig. 5, the variation in AOD was comparable with that of $PM_{2.5}$ concentrations (Fig. 2), and was consistent at all three sites during this study period (the missing AOD data were due to the accumulation of cloud).

In general, there were three serious air pollution episodes at all three sites around the holiday period. The background values of AOD at CAMS and Xianghe were similar, at about 0.45, and their α values were about 0.91 and 1.06, respectively. This indicates that fine-mode particles were dominant at these two sites (> 0.8). The AOD variation at Shangdianzi station was consistent with those at CAMS and Xianghe, but the values were systematically lower than those at the urban and suburban sites, suggesting there are fewer anthropogenic pollution sources in this region. The AOD and α background values were ~0.24 and 0.78, respectively, reflecting the dominance of coarse-mode particles at Shangdianzi.

It is clear that a serious pollution episode before the holiday also took place around 29 January. The maximum AOD and α values at CAMS, Xianghe and Shangdianzi all exceeded 1.50 and 1.3, suggesting significant formations of fine particles. This may have been because companies, industries and government usually give their employees leave about one week before the holiday officially begins, and higher traffic volumes are often seen at this time (Huang *et al.*, 2012; Jiang *et al.*, 2015).

During the holiday period, strongly increasing trends in AOD and α were observed. It should be noted that during the early three days of the holiday (7–9 February), the AODs were lower than the background level. As seen in Fig. 3, the strong northerly wind (~6 m $s^{-1}$) and relatively high PBLH (~550 m) favored the diffusion of air pollutants, contributing to better air quality. The strongly increasing trends in AOD were observed at all sites from 8 to 12 February. The peak AODs at CAMS and Xianghe occurred on 12 February, with values of ~1.62 and ~1.73, which were about 2.6 and 2.9 times higher than the background levels, respectively. The maximum at Shangdianzi was observed on 10 February, with a value of ~0.74, and was 2.1 times higher than the background level. The daily α values during this stage were seen to increase with the AODs and were almost higher than the background level. The peak values all exceeded 1.5, which suggested substantial generation of fine particles. The firework displays may have been responsible for the burst of heavy air pollution, as mentioned above. The intensive and widespread use of fireworks emits considerably high levels of pollutant gases (i.e., CO, $SO_2$, $NO_x$) (Wang *et al.*, 2007; Shi *et al.*, 2011) and, additionally, the humid environment (Fig. 2) would have greatly enhanced the formation of secondary organic aerosol species, leading to further deterioration in air quality (Blando *et al.*, 2000; Hennigan *et al.*, 2008). In summary, the mean values of AOD during this holiday period at CAMS, Xianghe and Shangdianzi were ~0.60, ~0.75 and ~0.29, which were 33%, 67% and 21% higher than background values, respectively. The averages of α at CAMS, Xianghe and Shangdianzi were ~1.21, ~1.17 and ~0.90, which were 34%, 10% and 13% higher than the background levels, respectively.

*SSA and Volume Size Distribution*

The SSA reflects the proportion of scattering by atmospheric aerosol particles in the total extinction and is one of the key variables for assessing the effects of aerosols on climate change. Fig. 6 shows the daily variation in SSA

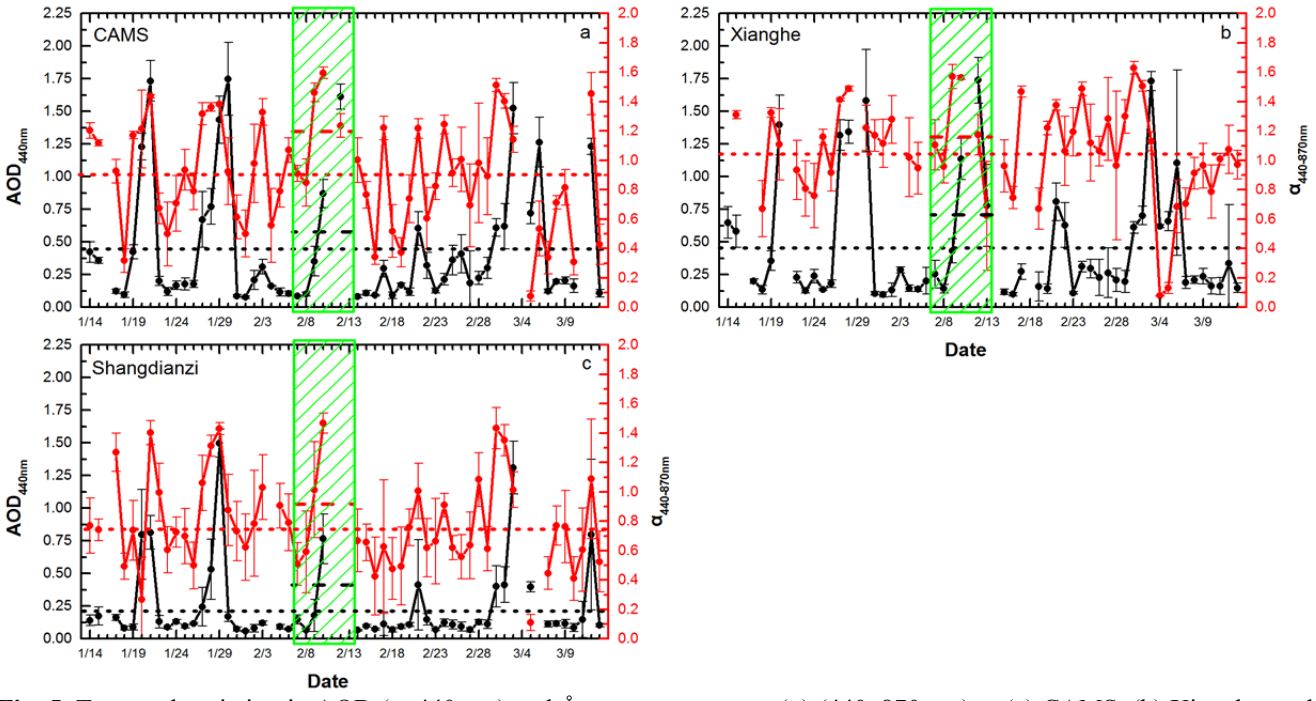


**Fig. 5.** Temporal variation in AOD (at 440 nm) and Ångström exponent (α) (440–870 nm) at (a) CAMS, (b) Xianghe, and (c) Shangdianzi.

at CAMS, Xianghe and Shangdianzi. Generally, the SSA background levels at 440 nm at CAMS, Xianghe and Shangdianzi were ~0.86, ~0.83 and ~0.84, while the holiday-mean SSA values were ~0.89, ~0.87 and ~0.86, which were about 3.5%, 5.0% and 2.4% higher than background values, respectively. These results suggest that the scattering by aerosol particles was enhanced during the holiday period.

On 7 February, the mean SSA values at 440 nm at CAMS, Xianghe and Shangdianzi were ~0.85, 0.86 and 0.83, respectively. As mentioned above, the favorable diffusion conditions contributed greatly to the better air quality, and these results were comparable with the value of 0.84 observed on a clean air day in Beijing (Jing *et al.*, 2011). It can be seen that the daily SSA values increased with AOD (Fig. 5) at the CAMS and Xianghe sites, especially during the most serious pollution stage (9–12 February). The maxima were observed on 12 February, with values of ~0.95 and ~0.96, which were about 10.5% and 15.7% higher than background levels, respectively. As mentioned above, firework displays contribute substantially to elevated atmospheric pollution (Wang *et al.*, 2007; Shi *et al.*, 2011), and increase the content of sulfates, nitrates and organic aerosols in the atmosphere, which are usually regarded as the main scattering aerosol particles (Drewnick *et al.*, 2005).

In addition, the spectral characteristics of the SSA are greatly affected by the size of aerosol particles. The RH was ~80% on 12 February, which may have greatly influenced the hygroscopic growth of water-soluble aerosols, enhancing the growth of fine-mode particles and resulting in a subsequent increase in the light scattering coefficient (Kotchenruther and Hobbs, 1998; Che *et al.*, 2014). In addition, the rate at which precursors to hygroscopic particles (e.g., sulfur and nitrogen oxides) were converted into sulfates and nitrates increased, resulting in substantial formation of secondary aerosols with strong scattering properties (Watson *et al.*, 1994; Tao *et al.*, 2014). These factors could be valid reasons for the extremely high SSA on 12 February.

Figs. 7(a)–7(c) show the variation in the particle size distribution at CAMS, Xianghe and Shangdianzi, respectively. The volume size distributions showed a bimodal logarithmic normal structure, with two peaks at radii of ~0.10–0.26 and ~2.30–3.50 μm, during the holiday period at the three sites.

It can be seen from Fig. 7(a) that the volume of the fine mode (radius < 0.60 μm) at this urban site during the holiday period was greater than the background level and showed an increasing trend, indicating the generation and accumulation of fine particles. The volume of fine-mode particles varied from 0.04 to 0.21 $\mu m^3\ \mu m^{-2}$, which was ~0.3 to 5.8 times more than the background level, respectively, and reached a peak on 12 February at a radius of 0.16 μm. As mentioned above, firework displays and high RH result in the formation of large numbers of fine particles (Wang *et al.*, 2007; Shi *et al.*, 2011). It should be noted that the aerosol radius corresponding to the maximum volume of fine-mode particles was bigger than those of pervious days (~0.12 μm), indicating the hygroscopic growth of fine particles should not be neglected.

From Fig. 7(b) we can see that during the most serious polluted period (9–12 February), the volume of fine particles at Xianghe gradually increased and reached a peak on 12 February, varying from 0.06 to 0.17 $\mu m^3\ \mu m^{-2}$, which was

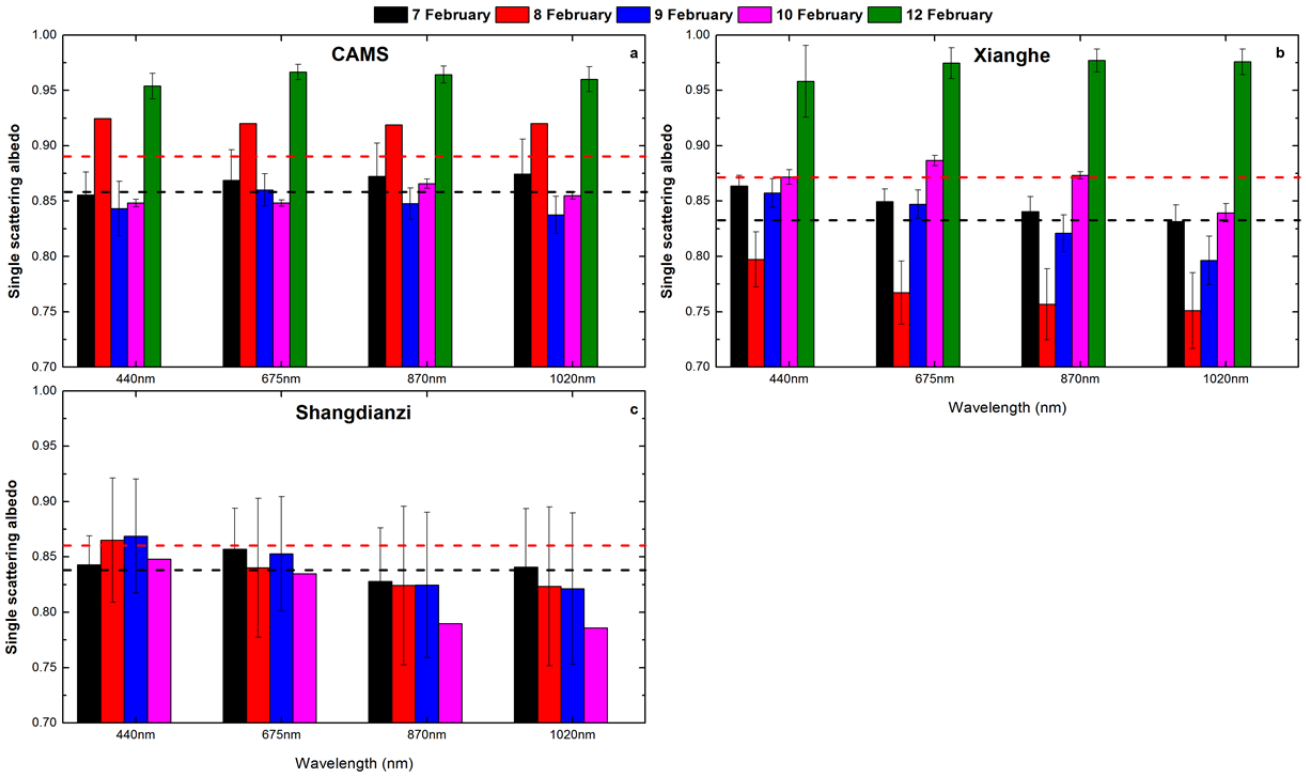


**Fig. 6.** Daily variation in SSA at (a) CAMS, (b) Xianghe, and (c) Shangdianzi.

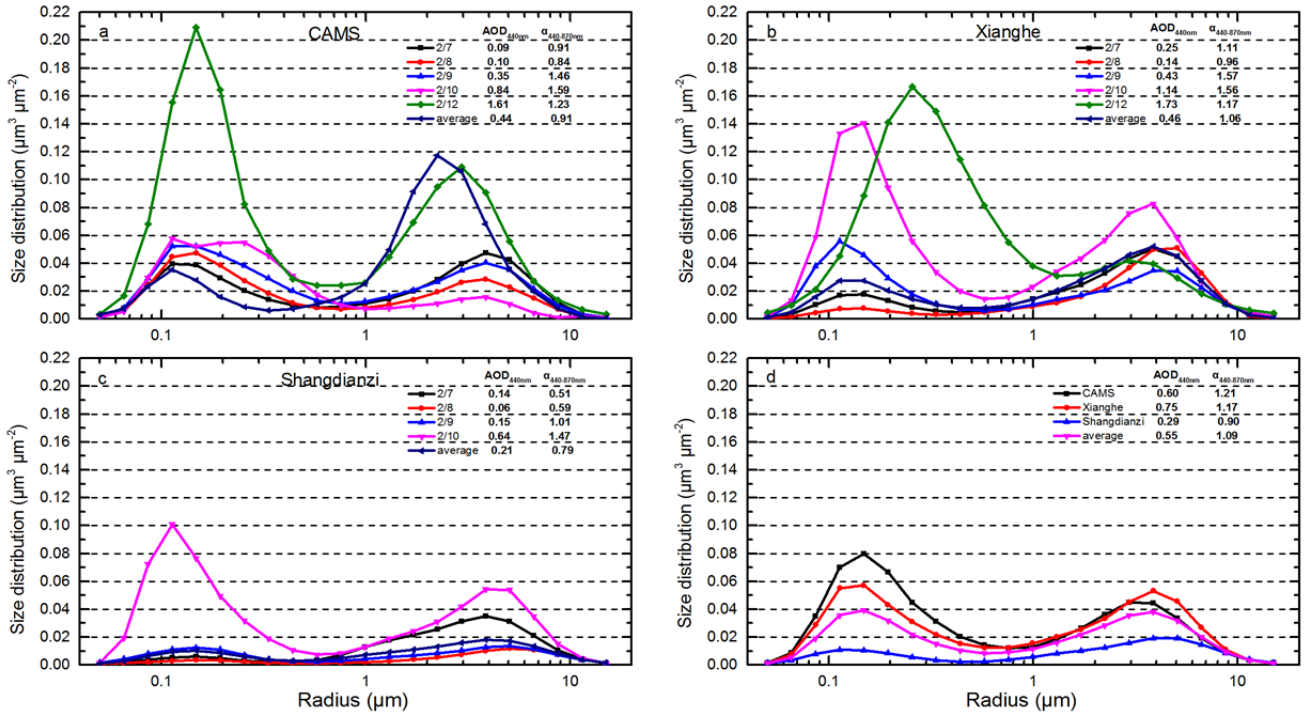


**Fig. 7.** Daily variation in size distributions of particulates at (a) CAMS, (b) Xianghe, and (c) Shangdianzi.

~1.1 to 4.7 times higher than the background value, respectively, indicating the generation of numerous fine particles. Similar to that of the CAMS site, the radius corresponding to the peak volume of fine-mode particles was also larger than those of other days, with a value of 0.26 μm, indicating the hygroscopic growth of fine particles.

It is clear that the total volumes of fine and coarse particles at Shangdianzi were relatively lower than those at the other two sites (Fig. 7(c)), indicating better atmospheric quality at this rural station due to there being fewer nearby pollution sources (Che *et al.*, 2014). However, during the intensive and widespread firework displays that occurred over the Beijing region for the Spring Festival holiday, the air pollution episode was seen. On 10 February, the volume of fine particles sharply increased and exceeded ~0.10 $\mu m^3\ \mu m^{-2}$, which was about 8.9 times higher than the background level. Similarly, the volume of coarse particles exceeded ~0.05, which was about 1.5 times higher than background level—probably resulting from the increasing content of fly ash derived from the explosion of fireworks (Yang *et al.*, 2009).

Fig. 7(d) compares the mean volume size distribution over CAMS, Xianghe, Shangdianzi, and their background levels. As can be seen, the mean volumes of fine and coarse particles at CAMS and Xianghe were all higher than the background levels, with values of (~0.08 $\mu m^3\ \mu m^{-2}$, ~0.05 $\mu m^3\ \mu m^{-2}$) and (~0.06 $\mu m^3\ \mu m^{-2}$, ~0.06 $\mu m^3\ \mu m^{-2}$), which were about (1.0, 0.5) and (0.3, 0.5) times higher than the background levels, respectively.

*AAOD and AAE*

The AAOD reflects the proportion of solar radiation absorbed by aerosol particles in the total extinction, the AOD, AAOD and AAE are related to one another as shown in Eqs. (1) and (2): (1) $AAOD(\lambda) = [1 - SSA(\lambda)] \times AOD(\lambda)$; (2) $AAE = -d\ln[AAOD(\lambda)/d\ln(\lambda)$. Fig. 8 shows the daily variations of AAOD and AAE (440–870 nm) at the three observation sites, and the missing date were result from the cloud accumulation and instrument problem. As demonstrated by many studies, the dust content, black carbon, and organic components are considered to be the main absorptive aerosols in the atmosphere (Russell *et al.*, 2010; Giles *et al.*, 2012), and the AAE has been widely used to classify the different types of these absorptive particles (Yang *et al.*, 2009; Gui *et al.*, 2016; Zheng *et al.*, 2017). Bergstrom (1973) and Bohren (2008) reported that the AAE value is close to 1.00 when black carbon dominates. A significant increase in organic aerosols leads to higher AAE values of between 1.00 and 2.00, due to the mixture of organic aerosols and strongly absorbing components in the atmosphere. Dust aerosols, which usually show strong absorptive capacity, result in an increase in AAE to between ~3.00 and ~5.00. An AAE value of < 1.00 indicates that the black carbon is coated with absorptive or non-absorptive materials for most of the time (Gyawali *et al.*, 2009).

In general, the air pollution episodes were all seen at the three sites during the Spring Festival holiday, characterized by sharply increasing AAOD values. The background values of AAOD at CAMS, Xianghe and Shangdianzi were ~0.05, ~0.06 and ~0.03, respectively. It should be noted that the background AAE at all sites was ~1.0, which means the dominant absorptive particles were black carbon.

During the holiday period, gradually increasing trends were seen in the variations of AAOD over CAMS, Xianghe and Shangdianzi, especially between 8 and 10 February. The AAOD varied from ~0.01 to ~0.13, ~0.03 to ~0.14, and ~0.01 to ~0.09 at CAMS, Xianghe, and Shangdianzi,

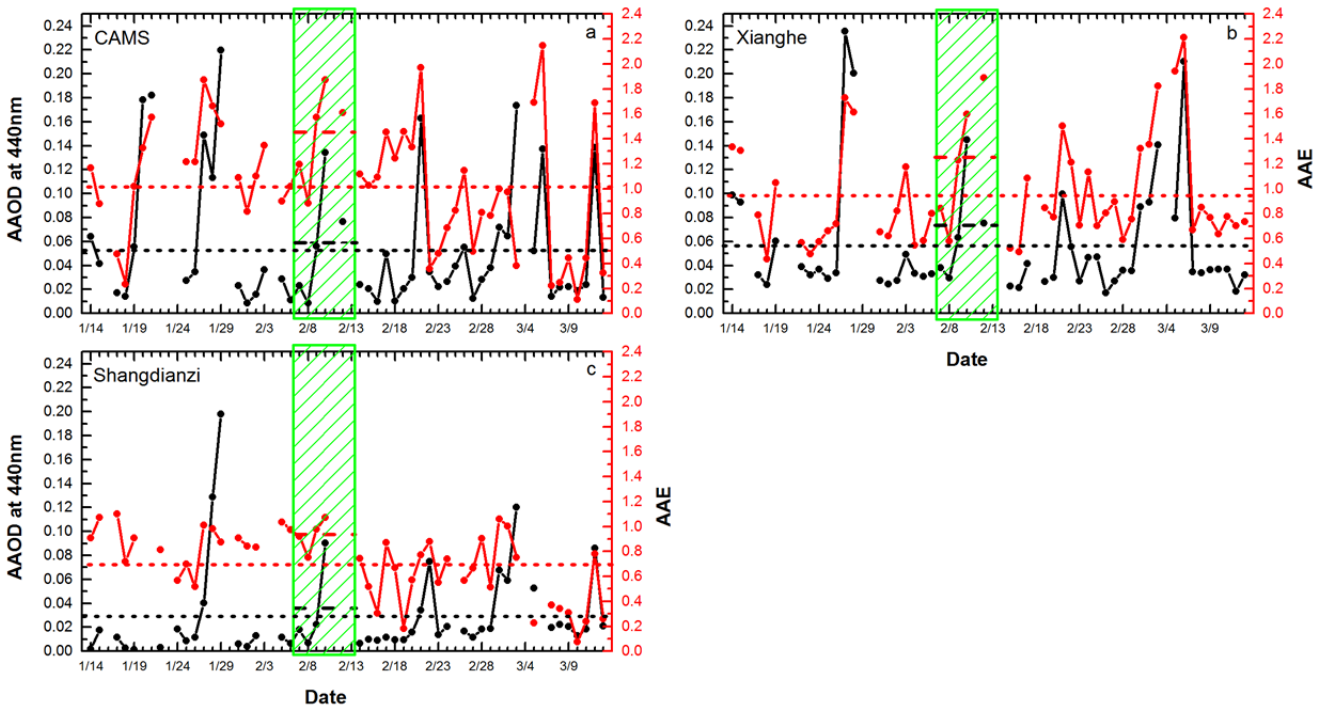


**Fig. 8.** Daily variation in AAOD and AAE at (a) CAMS, (b) Xianghe, and (c) Shangdianzi.

respectively. The peak AAOD values at these three sites were ~1.6, ~1.3 and ~2.0 times higher than the background levels, respectively, indicating more absorptive aerosol particles in the atmosphere—probably due to the firework displays (Huang *et al.*, 2012). The variations in AAE over CAMS and Xianghe were comparable, as illustrated by the coincident increasing trends with AAOD in Figs. 8(a) and 8(b). From 9 till 12 February especially, the AAEs all exceeded 1.00 and even reached ~2.00, indicating a significant increase in organic aerosols. These results were comparable with many other studies (Zheng *et al.*, 2017), suggesting that these secondary aerosols originating from fireworks were responsible for the intense air pollution during the Spring Festival holiday. In contrast, the AAE at Shangdianzi showed a slight variation during the holiday period, with a value of ~1.00, suggesting that black carbon dominated. In summary, the AAOD mean values during the holiday at CAMS, Xianghe and Shangdianzi were ~0.06, ~0.07 and ~0.04, which were about 20.0%, 16.7% and 33.3% higher than background levels, respectively. At CAMS and Xianghe, organic particles dominated the aerosol absorption, while black carbon was responsible for the high absorptive aerosol content at Shangdianzi.

*Aerosol Radiative Forcing*

The aerosol radiative forcing (ARF) demonstrates the actual or total radiative impacts caused by atmospheric aerosols, which is key to evaluating regional and global climate change (García *et al.*, 2012).

Figs. 9(a) and 9(c) show the daily variation in ARF at the surface (ARF-BOA) and at the top of the atmosphere (ARF-TOA) at each site. Fig. 9(e) presents the mean heating effect of ARF on the atmosphere during the Spring Festival holiday. As the pollution episode developed, the values of ARF-BOA at all sites increased (Fig. 9(a)). On the most polluted day over the Beijing region (12 February), peak ARF-BOA values were observed at CAMS and Xianghe, exceeding –130 and –150 W $m^{-2}$, respectively, whereas the maximum ARF-BOA value was found on 10 February, with a mean value of about –110 W $m^{-2}$. The daily averages of ARF-BOA varied from –20 to –130, –40 to –150, and –10 to –110 W $m^{-2}$ at CAMS, Xianghe, and Shangdianzi, respectively. It should be noted that the mean value for these three sites during the holiday was –70 W $m^{-2}$, which was about 27.3% higher than the background level, indicating that the cooling effect produced by aerosol particles was enhanced (Che *et al.*, 2014).

The variations in ARF-TOA showed similar trends to the ARF-BOA at the three stations during the holiday period (Fig. 9(c)). The daily averages varied from –5 to –80, –3 to –85, and –2 to –20 W $m^{-2}$ at CAMS, Xianghe, and Shangdianzi, respectively. The average value for the three sites was –25 W $m^{-2}$, which was about 66.7% greater than background level, indicating that the aerosol particles imposed a cooling effect at the TOA during the holiday.

It can be seen from Fig. 9(e) that the heating effects on the atmosphere varied from 10 to 70, 35 to 110, and 5 to 90 W $m^{-2}$ at CAMS, Xianghe, and Shangdianzi, respectively. The mean value for the three sites was ~50 W $m^{-2}$, which was about 25% higher than the background level during the holiday. These results illustrate that the higher absorbing capacity of atmospheric aerosol particles reduced the solar radiation backscattering to the TOA, and a larger percentage of solar energy was retained in the atmosphere over the Beijing region, suggesting that the atmosphere was strongly heated by ARF during the Spring Festival holiday.

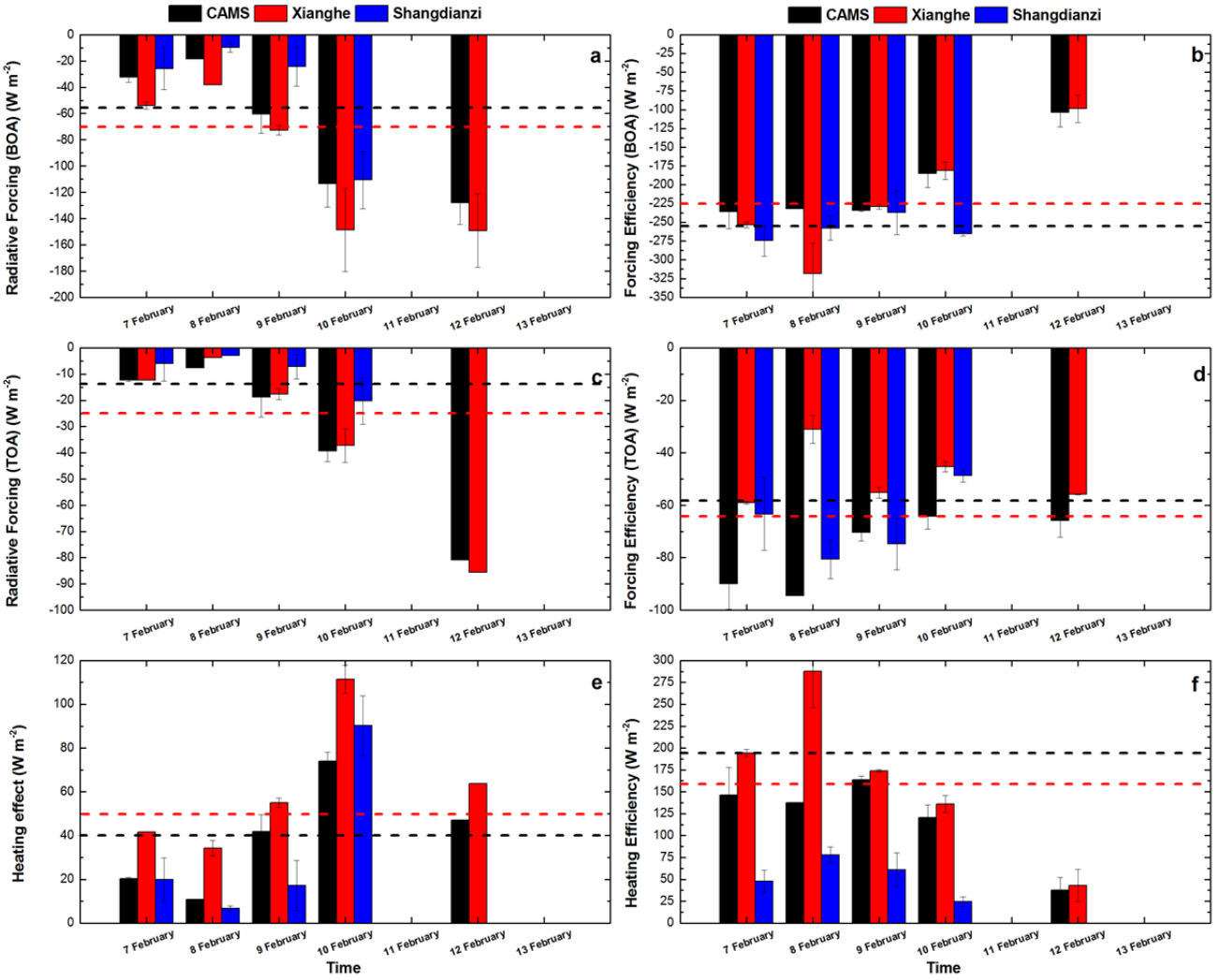


**Fig. 9.** (a, c, e) Aerosol radiative forcing at the surface (bottom of the atmosphere; BOA), at the top of the atmosphere (TOA), and the heating effect, and (b, d, f) their efficiencies at CAMS, Xianghe, and Shangdianzi.

Che *et al.* (2014) reported that ARF efficiency is a more appropriate variable to make a consistent comparison among the ARF of atmospheric aerosols, and this is defined as the rate of atmospheric forcing per unit of AOD. The daily variation in the forcing efficiency at the BOA varied from –100 to –240, –100 to –340, and –240 to –275 W $m^{-2}$ at CAMS, Xianghe, and Shangdianzi, respectively, as Fig. 9(b) shows. The mean value for the three sites was –225 W $m^{-2}$, which was about 10.0% less than the background level during the holiday—probably due to the higher SSA value during the holiday period (Che *et al.*, 2014). In Fig. 9(d), we can see that the ARF-TOA efficiencies at CAMS, Xianghe, and Shangdianzi varied from –65 to –90, –30 to –60, and –50 to –80 W $m^{-2}$, respectively. The average was –65 W $m^{-2}$, which was about 12.1% higher than the background level, because a higher AOD induces a larger ARF (Xia *et al.*, 2007). The heating efficiency varied from –40 to –185, –50 to –289, and –25 to –75 W $m^{-2}$ at CAMS, Xianghe, and Shangdianzi, respectively, as Fig. 9(f) demonstrates. The mean value was –160 W $m^{-2}$, which was about 18.8% less than the background level, and which could have been related to the sharp increase in AOD during the holiday (Che *et al.*, 2014).

### *PSCF and CWT Analysis*

PSCF analysis was conducted in this study to investigate the potential source regions of the atmospheric pollutants over Beijing during the holiday period using TrajStat (Wang *et al.*, 2009). The averages of hourly data from all environmental monitoring stations in the Beijing region, along with the corresponding 72-h back-trajectories at an altitude of 500 m, were used as the input for the PSCF model. In this study, the PSCF values were calculated using the Class II Chinese standard (< 75 μg $m^{-3}$, GB 3095–2012: http://kjs.mep.gov.cn/hjbhbz/bzwb/dqhjbh/dqhjzlbz/201203/t20120302_224165.shtml) as the criterion. The results for the particle mass concentrations ($PM_{2.5}$) are shown in Fig. 10(a).

As can be seen, the high PSCF values were mainly located south of Beijing, such as the south part of Hebei and Shanxi provinces, and the central northern part of Shandong province. This finding is comparable to other studies (Xia *et al.*, 2007; Yan *et al.*, 2015; Zheng *et al.*, 2017) and

consistent with the results above. Hebei, Shanxi, and Shandong are usually regarded as industrial and agricultural provinces, and are highly polluted. During the holiday, the atmospheric pollutants originating from these areas were transported by southerly winds (as Figs. 2 and 3 show) and arrived later in Beijing, largely contributing to the severe air pollution episodes. It should be noted that the northwestern part of Beijing also showed other influences on the air pollution in Beijing, such as the central and eastern regions of Inner Mongolia, suggesting that atmospheric pollution in Beijing is partially caused by long-range transport from these upstream areas in winter (such as fine dust particles) (Wehner *et al.*, 2008).

CWT analysis was employed to explore the relative contribution of each potential source area to the high pollutant loadings in Beijing. As can be seen from Fig. 10(b), the distribution of CWT values was comparable to that of PSCF, with high CWT values also located south of Beijing, such as the southern regions of Hebei and Shanxi provinces and the northern region of Shandong province. The contribution of these potential source regions to the $PM_{2.5}$ loadings in Beijing varied from 70 to 130 μg $m^{-3}$, and even exceeded 150 μg $m^{-3}$ in some areas. Compared with the south of Beijing, the contributions from the north of Beijing were relative low, varying from 30 to 90 μg $m^{-3}$ in the central and eastern regions of Inner Mongolia. It should be noted that the local emissions of air pollutants contributed to the extremely high particle loading to some degree, contributing values of about 50 to 110 μg $m^{-3}$, and indicating that local emissions of atmospheric pollutants (such as fireworks during the holiday) need to be given consideration (Zhang *et al.*, 2009; Zhu *et al.*, 2014; Zheng *et al.*, 2016).

## CONCLUSIONS

A comparative analysis of the microphysical and optical properties, and radiative forcing of aerosols was conducted between three stations with different underlying surface conditions during the Spring Festival in Beijing using ground-based data, meteorological observations, and atmospheric environmental monitoring data.

Aside from natural emission sources, the meteorological conditions contributed greatly to the severe air pollution during the holiday. The high RH and unfavorable diffusion conditions (weak southerly winds, a decreasing boundary layer height, and surface temperature inversion) were favorable to the accumulation and significant increase in atmospheric pollutants ($PM_{2.5}$).

The aerosol optical properties based on ground measurements showed that the AOD at 440 nm consistently varied at CAMS, Xianghe, and Shangdianzi, illustrating the fact that severe air pollution partially caused by fireworks is a regional phenomenon over this megacity. During the air-pollution period (8–12 February), the AOD increased at CAMS, Xianghe, and Shangdianzi, with daily peak values of ~1.62, ~1.73, and ~0.74, which were about 2.6, 2.9, and 2.1 times higher than the background levels, respectively. During the most polluted periods, α was usually > 1.40, suggesting that substantial formations of small particles contributed greatly to this air-pollution episode.

The SSA increased with the AOD during the most polluted periods, especially under conditions of high RH. The peak values of daily SSA at CAMS, Xianghe, and Shangdianzi were ~0.95, ~0.96, and ~0.87. The size distribution showed an obvious bimodal logarithmic normal structure, with two peaks at radii of ~0.10–0.26 and ~2.30–3.50 μm during the holiday period at all three sites. An increased volume of fine-mode particles was found at all the sites and varied from 0.04 to 0.21 $\mu m^3$ $\mu m^{-2}$, 0.06 to 0.17 $\mu m^3$ $\mu m^{-2}$, and 0.01 to 0.10 $\mu m^3$ $\mu m^{-2}$, which was about 0.3 to 5.8, 1.1 to 4.7, and 1.2 to 8.9 times higher than the background values of CAMS, Xianghe, and Shangdianzi, respectively, indicating the contribution of fine mode particles. The daily AAOD varied from ~0.01 to ~0.13, ~0.03 to ~0.14, and ~0.01 to ~0.09 at CAMS, Xianghe, and Shangdianzi, respectively. During the most polluted period, the AAEs all exceeded 1.00 and even reached ~2.00 at CAMS and Xianghe, indicating a significant increase in organic aerosols, while the AAEs at Shangdianzi remained at ~1.00, meaning that black carbon was responsible for the high AAOD values.

The daily ARF-BOA varied from –20 to –130, –40 to –150, and –10 to –110 W $m^{-2}$ during the holiday at CAMS, Xianghe, and Shangdianzi, respectively. The ARF-TOA showed similar trends to the ARF-BOA and varied from –5 to –80, –3 to –85, and –2 to –20 W $m^{-2}$ for CAMS, Xianghe,

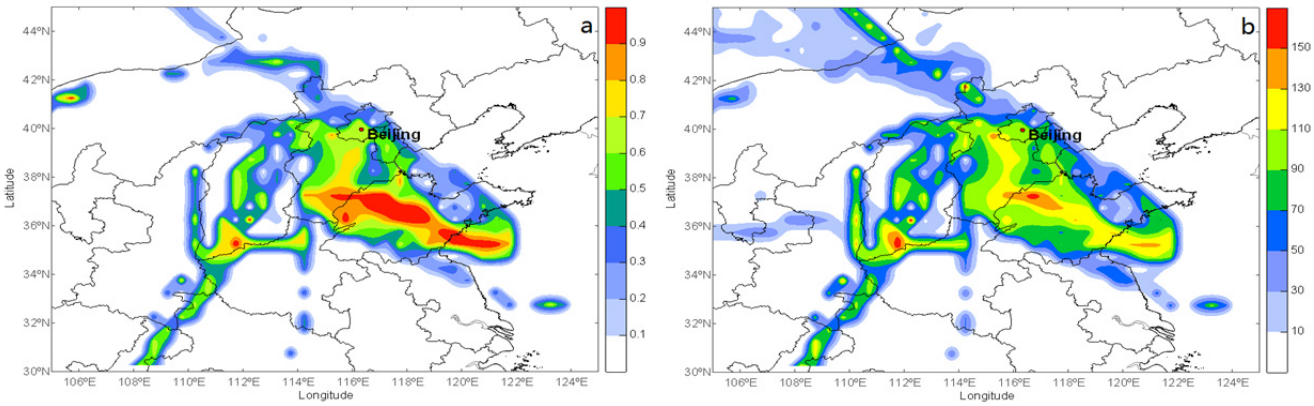


**Fig. 10.** Results of the (a) PSCF, and (b) CWT analyses during the holiday period in Beijing.

and Shangdianzi, respectively. The daily heating effect of ARF varied from 10 to 70, 35 to 110, and 5 to 90 W $m^{-2}$ for CAMS, Xianghe, and Shangdianzi, respectively. The mean value for the three sites was ~50 W $m^{-2}$, which was about 25% higher than the background level during the holiday, suggesting that the atmosphere was strongly heated by ARF.

The PSCF and CWT analyses showed that Beijing, the southern parts of Hebei and Shanxi Provinces, and the central northern part of Shandong Province were responsible for the extremely high $PM_{2.5}$ particle loading. The contribution values were about 50 to 110, 70 to 130, and 30 to 90 μg $m^{-3}$, respectively, indicating that the air pollution is a regional problem.

This study investigated the relationship between meteorological factors and aerosol optical properties during a pollution episode over Beijing during the Spring Festival. More detailed information on the microphysical processes, mechanisms of influence, and chemical composition of air pollutants still needs to be obtained through further observations or numerical simulations for the sake of improving regional air quality.

## ACKNOWLEDGEMENTS

This work was supported by a grant from the National Key R & D Program Pilot Projects of China (2016YFA0601901), the National Natural Science Foundation of China (41590874, 41475138 & 41375153), the Natural Science Foundation of Zhejiang Province (LY16010006), the CAMS Basis Research Project (2016Z001, 2014R17 & 2017Z011), the Climate Change Special Fund of CMA (CCSF201504), the Special Project of Doctoral Research supported by Liaoning Provincial Meteorological Bureau (D201501), the Hangzhou Science and Technology Innovative project (20150533B17) and the European Union Seventh Framework Programme (FP7/2007–2013) under grant agreement no. 262254. The authors would like to thank the three anonymous reviewers and the editor for their constructive suggestions and comments.

## REFERENCE

Ackerman, T. and Toon, O. (1981). Absorption of visible radiation in atmosphere containing mixtures of absorbing and nonabsorbing particles. *Appl. Opt.* 20: 3661–3668.

Bergstrom, R. (1973). Extinction and absorption coefficients of the atmospheric aerosol as a function of particle size. *Contr. Atmos. Phys*. 46: 223–234.

Blando, J. and Turpin, B. (2000). Secondary organic aerosol formation in cloud and fog droplets: A literature evaluation of plausibility. *Atmos. Environ.* 34: 1623–1632.

Bohren, C. and Huffman, D. (2008). *Absorption and scattering of light by small particles*. John Wiley & Sons.

Charlson, R. and Schwartz, S. (1992). Climate forcing by anthropogenic aerosols. *Science* 255: 423–430.

Che, H., Shi, G., Zhang, X., Arimoto, R., Zhao, Q., Xu, L., Wang, B. and Chen, H. (2005). Analysis of 40 years of solar radiation data from China, 1961–2000. *Geophys. Res. Lett*. 32: L06803.

Che, H., Zhang, X., Li, Y., Zhou, Z. and Qu, J. (2007). Horizontal visibility trends in China 1981–2005. *Geophys. Res. Lett*. 34: L24706.

Che, H., Shi, G., Uchiyama, A., Chen, H., Goloub, P. and Zhang, Z. (2008). Intercomparison between aerosol optical properties by a PREDE skyradiometer and CIMEL sunphotometer over Beijing, China. *Atmos. Chem. Phys*. 8: 3199–3214.

Che, H., Xia, X., Zhu, J., Dubovik, O., Holben, B., Goloub, P., Chen, H., Estelles, V., Wang, H., Zhao, H., Zhang, X., Wang, Y., Sun, J., Tao, R. and Shi, G. (2014). Column aerosol optical properties and aerosol radiative forcing during a serious haze-fog month over North China Plain in 2013 based on ground-based sunphotometer measurements. *Atmos. Chem. Phys*. 14: 2125–2138.

Che, H., Xia, X., Zhu, J., Wang, H., Wang, Y., Sun, J., Zhang, X. and Shi, G. (2015). Aerosol optical properties under the condition of heavy haze over an urban site of Beijing, China. *Environ. Sci. Pollut. Res*. 22: 1043–1053.

Che, H., Qi, B., Zhao, H., Xia, X., Eck, T., Goloub, P., Dubovik, O., Estelles, V., Wu, Y., Zhu, J., Wang, H., Gui, K., Yu, J., Zheng, Y., Sun, T., Chen, Q., Shi, G. and Zhang, X. (2018). Aerosol optical properties and direct radiative forcing based on measurements from the China Aerosol Remote Sensing Network (CARSNET) in eastern China. *Atmos. Chem. Phys.* 18: 405–425.

Chen, J., Xin, J., An, J., Wang Y., Liu, Z., Chao, N. and Meng, Z. (2014). Observation of aerosol optical properties and particulate pollution at background station in the Pearl River Delta region. *Atmos. Res*. 143: 216–227.

Deardorff, J. (1972). Parameterization of the planetary boundary layer for use in general circulation models. *Mon. Weather Rev.* 100: 93–106.

Draxler, R. and Hess, G. (1998). An overview of the HYSPLIT_4 modelling system for trajectories. *Aust. Meteorol. Mag.* 47: 295–308.

Drewnick, F., Hings, S., Curtius, J., Eerdekens, G. and Williams, J. (2006). Measurement of fine particulate and gas-phase species during the New Year's fireworks 2005 in Mainz, Germany. *Atmos. Environ*. 40: 4316–4327.

Dubovik, O. and King, M. (2000). A flexible inversion algorithm for retrieval of aerosol optical properties from Sun and sky radiance measurements. *J. Geophys. Res*. 105: 20673–20696.

Eck, T., Holben, B., Sinyuk, A., Pinker, R., Goloub, P., Chen, H., Chatenet, B., Li, Z., Tripath, S., Reid, J., Giles, D., Dubovik, O., Smirnov, A., Wang, P. and Xia, X. (2010). Climatological aspects of the optical properties of fine/coarse mode aerosol mixtures. *J. Geophys. Res.* 115: D19205.

Eck, T., Holben, B., Reid, J., Giles, D., Rivas, M., Singh, R., Dubovik, O., Carn, S., Sinyuk, A., Arola, A., Smirnov, A., Chen, H. and Goloub, P. (2012). Fog-and cloud-induced aerosol modification observed by the Aerosol Robotic Network (AERONET). *J. Geophys. Res.* 117: D07206.

Fu, G., Xu, W., Yang, R., Li, J. and Zhao, C. (2014). The distribution and trends of fog and haze in the North

China plain over the past 30 years. *Atmos. Chem. Phys*. 14: 11949–11958.

Gao, Y., Zhang, M., Liu, Z., Wang, L., Wang, P., Xia, X., Tao, M. and Zhu, L. (2015). Modeling the feedback between aerosol and meteorological variables in the atmospheric boundary layer during a severe fog-haze event over the North China Plain. *Atmos. Chem. Phys*. 15: 1093–1130.

Garland, R., Yang, H., Schmid, O., Rose, D., Nowak, A., Takegawa, M., Kita, K., Kondo, Y., Shao, M., Zeng, L. and Zhang, H. (2008). Aerosol optical properties in a rural environment near the mega-city Guangzhou, China: Implications for regional air pollution, radiative forcing and remote sensing. *Atmos. Chem. Phys*. 8: 5161–5186.

Ge, J., Su, J., Ackerman, T., Fu, Q. and Shi, S. (2010). Dust aerosol optical properties retrieval and radiative forcing over northwestern China during the 2008 China-US joint field experiment. *J. Geophys. Res.* 115: D00K12.

Giles, D., Holben, B., Eck, T., Sinyuk, A., Dickerson, R., Thompson, A. and Schafer, J. (2012). An analysis of AERONET aerosol absorption properties and classifications representative of aerosol source regions. *J. Geophys. Res*. 117: D17203.

Gui, K., Che, H., Chen, Q., An, L., Zeng, Z., Guo, Z., Zheng, Y., Wang, H., Yu, J. and Zhang, X. (2016). Aerosol optical properties based on ground and satellite retrievals during a serious haze episode in December 2015 over Beijing. *Atmosphere* 7: 70.

Gui, K., Che, H., Chen, Q., Zeng, Z., Zheng, Y., Long, Q., Sun, T., Wang, Y. and Zhang, X. (2017). Water vapor variation and the effect of aerosols in China. *Atmos. Environ*. 165: 322–335.

Gyawali, M., Arnott, W., Lewis, K. and Moosmüller, H. (2009). In situ aerosol optics in Reno, NV, USA during and after the summer 2008 California wildfires and the influence of absorbing and non-absorbing organic coatings on spectral light absorption. *Atmos. Chem. Phys*. 9: 8007–8015.

Hansen, J., Sato, M., Ruedy, R. and Oinas, V. (2000). Global warming in the twenty-first century: An alternative scenario. *Proc. Natl. Acad. Sci. U.S.A*. 97: 9875–9880.

Hennigan, C., Bergin, M. and Dibb, J. (2008). Enhanced secondary organic aerosol formation due to water uptake by fine particles. *Geophys. Res. Lett*. 35: L18801.

Holben, B., Eck, T., Slutsker, I., Buis, J., Setzer, A., Lavenu, F. and Smirnov, A. (1998). AERONET—A federated instrument network and data archive for aerosol characterization. *Remote Sens. Environ*. 66: 1–16.

Hsu, Y., Holsen, T. and Hopke, P. (2003). Comparison of hybrid receptor models to locate PCB sources in Chicago. *Atmos. Environ*. 37: 545–562.

Huang, K., Zhuang, G., Lin, Y., Wang, Q., Fu, J., Zhang, R., Li, J. and Fu, Q. (2012). Impact of anthropogenic emission on air quality over a megacity–revealed from an intensive atmospheric campaign during the Chinese Spring Festival. *Atmos. Chem. Phys*. 12: 11631–11645.

Jiang, Q., Sun, Y., Wang, Z. and Yin, L. (2015). Aerosol composition and sources during the Chinese Spring Festival: Fireworks, secondary aerosol, and holiday effects. *Atmos. Chem. Phys*. 15: 6023–6034.

Jing, H., Li, Y., Zhao, J., Li, B., Chen, R., Gao, Y. and Chen, C. (2014). Wide-range particle characterization and elemental concentration in Beijing aerosol during the 2013 Spring Festival. *Environ. Pollut*. 192: 204–211.

Kotchenruther, R. and Hobbs, P. (1998). Humidification factors of aerosols from biomass burning in Brazil. *J. Geophys. Res*. 103: 32081–32089.

Leng, C., Duan, J., Xu, C., Zhang, H., Zhang, Q., Wang, Y., Li, X. and Chen, J. (2015). Insights into a historic severe haze weather in Shanghai: Synoptic situation, boundary layer and pollutants. *Atmos. Chem. Phys*. 16: 9221–9234.

Li, Z., Gu, X., Wang, L., Xie, Y., Dubovik, O., Schuster, G., Goloub, P., Li, L. and Xu, H. (2013). Aerosol physical and chemical properties retrieved from ground-based remote sensing measurements during heavy haze days in Beijing winter. *Atmos. Chem. Phys*. 13: 10171–10183.

Luo, Y., Lu, D., Zhou, X., Li, W. and He, Q. (2001). Characteristics of thespatial distribution and yearly variation of aerosol optical depth over China in last 30 years. *J. Geophys. Res*. 106: 14501–14513.

Polissar, A., Hopke, P. and Harris, J. (2001). Source regions for atmospheric aerosol measured at Barrow, Alaska. *Environ. Sci. Technol*. 35: 4214–4226.

Qiu, J. and Yang, L. (2000). Variation characteristics of atmospheric aerosol optical depths and visibility in North China during 1980–1994. *Atmos. Environ*. 34: 603–609.

Ramanathan, V., Crutzen, P., Lelieveld, J., Mitra, P., Chung, C, Clarke, A., Collins, W., Hudson, J. and Valero, F. (2001). Indian Ocean Experiment: An integrated analysis of the climate forcing and effects of the great Indo-Asian haze. *J. Geophys. Res*. 106: 28371–28398.

Russell, P., Bergstrom, R., Shinozuka, Y., Clarke, A., DeCarlo, P., Dubovik, O. and Strawa, A. (2010). Absorption Angstrom Exponent in AERONET and related data as an indicator of aerosol composition. *Atmos. Chem. Phys*. 10: 1155–1169.

Shi, Y., Zhang, N., Gao, J., Lin, X. and Cai, Y. (2011). Effect of fireworks display on perchlorate in air aerosols during the Spring Festival. *Atmos. Environ*. 45: 1323–1327.

Stohl, A. (1996). Trajectory statistics — a newmethod to establish source–receptor relationships of air pollutants and its application to the transport of particulate sulfate in Europe. *Atmos. Environ*. 30: 579–587.

Tao, M., Chen, L., Wang, Z., Ma, P., Tao, J. and Jia, S. (2014). A study of urban pollution and haze clouds over northern China during the dusty season based on satellite and surface observations. *Atmos. Environ*. 82: 183–192.

Wang, J. and Christopher, S. (2003). Intercomparison between satellite-derived aerosol optical thickness and $PM_{2.5}$ mass: Implications for air quality studies. *Geophys. Res. Lett*. 30: 2095.

Wang, X., Huang, J., Ji, M. and Higuchi, K. (2008). Variability of East Asia dust events and their long-term trend. *Atmos. Environ*. 42: 3156–3165.

Wang, X., Huang, J., Zhang, R., Chen, B. and Bi, J. (2010). Surface measurements of aerosol properties over northwest

China during ARM China 2008 deployment. *J. Geophys. Re.* 115: D00K27.

Wang, Y., Zhuang, G., Sun, Y. and An, Z. (2006). The variation of characteristics and formation mechanisms of aerosols in dust, haze, and clear days in Beijing. *Atmos. Environ.* 40: 6579–6591.

Wang, Y., Zhuang, G., Xu, C. and An, Z. (2007). The air pollution caused by the burning of fireworks during the lantern festival in Beijing. *Atmos. Environ*. 41: 417–431.

Wang, Y., Zhang, X. and Draxler, R. (2009). TrajStat: GIS-based software that uses various trajectory statistical analysis methods to identify potential sources from long-term air pollution measurement data. *Environ. Modell. Software* 24: 938–939.

Wang, Y., Xin, J., Li, Z., Wang, S., Wang, P., Hao, W., Nordgren, B., Chen, H. and Sun, Y. (2011). Seasonal variations in aerosol optical properties over China. *J. Geophys. Res*. 116: D18209.

Wang, Y., Yao, L., Wang, L., Liu, Z., Ji, D., Tang, G., Zhang, J. and Xin, J. (2014). Mechanism for the formation of the January 2013 heavy haze pollution episode over central and eastern China. *Sci. China Earth Sci*. 57: 14–25.

Watson, J., Chow, J., Lurmann, F. and Musarra, S. (1994). Ammonium nitrate, nitric acid, and ammonia equilibrium in wintertime Phoenix. Arizona. *Air Waste* 44: 405–412.

Watson, J. (2002). Visibility: Science and regulation. *J. Air Waste Manage. Assoc.* 52: 628–713.

Wehner, B., Birmili, W., Ditas, F., Wu, Z, Liu, X., Sugimoto, N. and Wiedensohler, A. (2008). Relationships between submicrometer particulate air pollution and air mass history in Beijing, China, 2004–2006. *Atmos. Chem. Phys*. 8: 6155–6168.

Xia, X., Chen, H., Wang, P., Zong, X., Qiu, J. and Gouloub, P. (2005). Aerosol Properties and their spatial and temporal variations over north China in spring 2001. *Tellus B* 57: 28–39.

Xia, X., Chen, H., Goloug, P., Zhang, W., Chatenet, B. and Wang, P. (2007). A compilation of aerosol optical properties and calculation of direct radiative forcing over an urban region in northern China. *J. Geophys. Res*. 112: D12203.

Xin, J., Zhang, Q., Wang, L., Gong, C., Wang, Y., Liu, Z. and Gao, W. (2014). The empirical relationship between the $PM_{2.5}$ concentration and aerosol optical depth over the background of North China from 2009 to 2011. *Atmos. Res*. 138: 179–188.

Xin, Y., Wang, G. and Chen, L. (2016). Identification of long-range transport pathways and potential sources of $PM_{10}$ in Tibetan Plateau uplift area: Case study of Xining, China in 2014. *Aerosol Air Qual. Res*. 16: 1044–1054.

Xue, M., Ma, J., Yan, P. and Pan, X. (2011). Impacts of pollution and dust aerosols on the atmospheric optical properties over a polluted rural area near Beijing city. *Atmos. Res*. 101: 835–843.

Yan, R., Yu, S., Zhang, Q., Li, P., Wang, S., Chen, B. and Liu, W. (2015). A heavy haze episode in Beijing in February of 2014: Characteristics, origins and implications. *Atmos. Pollut. Res*. 6: 867–876.

Yang, M., Howell, S., Zhuang, J. and Huebert, B. (2009). Attribution of aerosol light absorption to black carbon, brown carbon, and dust in China – interpretations of atmospheric measurements during EAST-AIRE. *Atmos. Chem. Phys*. 9: 2035–2050.

Yu, X., Shi, C., Ma, J., Zhu, B, Li, M., Wang, J., Yang, S. and Kang, N. (2013). Aerosol optical properties during firework, biomass burning and dust episodes in Beijing. *Atmos. Environ*. 81: 475–484.

Yu, X., Kumar, K., Lü, R. and Ma, J. (2016). Changes in column aerosol optical properties during extreme haze-fog episodes in January 2013 over urban Beijing. *Environ. Pollut*. 210: 217–226.

Zhang, J., Sun, Y., Liu, Z., Ji, D. and Wang, Y. (2009). Characterization of submicron aerosols during a serious pollution month in Beijing (2013) using an aerodyne high-resolution aerosol mass spectrometer. *Atmos. Chem. Phys. Discuss.* 13: 19009–19049.

Zhang, R., Jing, J., Tao, J., Hsu, S., Wang, G, Cao, J., Lee, C., Zhu, L., Chen, Z., Zhao, Y. and Shen, Z. (2013). Chemical characterization and source apportionment of $PM_{2.5}$ in Beijing: Seasonal perspective. *Atmos. Chem. Phys*. 13: 7053–7074.

Zhang, R., Khalizov, A., Pagels, J., Zhang, D., Xue, H. and McMurry, P. (2008). Variability in morphology, hygroscopicity, and optical properties of soot aerosols during atmospheric processing. *Proc. Natl. Acad. Sci. U.S.A.* 105: 10291–10296.

Zhao, X., Zhang, X., Xu, X., Xu, J., Yang, M. and Pu, W. (2009). Seasonal and diurnal variations of ambient $PM_{2.5}$ concentration in urban and rural environments in Beijing. *Atmos. Environ*. 43: 2893–2900.

Zheng, Y., Che, H., Zhao, T., Xia, X., Gui, K., An, L., Qi, B., Wang, H., Wang, Y., Yu, J. and Zhang, X. (2016). Aerosol optical properties over Beijing during the world athletics championships and victory day military parade in August and September 2015. *Atmosphere* 7: 47.

Zheng, Y., Che, H., Zhao, T., Zhao, H., Gui, K., Sun, T., An, L., Yu, J., Liu, C., Jiang, Y., Zhang, L., Wang, H., Wang, Y. and Zhang, X. (2017). Aerosol optical properties observation and its relationship to meteorological conditions and emission during the Chinese National Day and Spring Festival holiday in Beijing. *Atmos. Res*. 197: 188–200.

Zhu, J., Che, H., Xia, X., Chen, H., Goloub, P. and Zhang, W. (2014). Column-integrated aerosol optical and physical properties at a regional background atmosphere in North China Plain. *Atmos. Environ*. 84: 54–64.

*Received for review, October 18, 2017*
*Revised, January 29, 2018*
*Accepted, February 7, 2018*